Pressure-induced proton transfer in cocrystals of glutaric acid and 4,4'-vinylenodipyridine

Ewa Patyk-Kaźmierczak,*[a] Fernando Izquierdo-Ruiz,[b] Alvaro Lobato,[b] Sebastiano Romi,[c,d] Michał Kaźmierczak,[a] Marcela Wątor,[a] Roberto Bini,[c,d,e] J. Manuel Recio.[f]

[a] Faculty of Chemistry, Adam Mickiewicz University in Poznań, Poznań, Poland.
[b] MALTA-Consolider Team and Departamento de Química Física, Complutense University of Madrid, Madrid, Spain.
[c] LENS, European Laboratory for Non-linear Spectroscopy, Sesto Fiorentino, Firenze, Italy
[d] Dipartimento di Chimica "Ugo Schiff", Università degli Studi di Firenze, Sesto Fiorentino, Firenze, Italy
[e] ICCOM-CNR, Institute of Chemistry of OrganoMetallic Compounds, National Research Council of Italy, Sesto Fiorentino, Firenze, Italy
[f] MALTA-Consolider Team and Departamento de Química Física y Analítica, University of Oviedo, Oviedo, Spain.

*corresponding author: Ewa Patyk-Kaźmierczak, Faculty of Chemistry, Adam Mickiewicz University in Poznań, Poznań, Poland; email: ewapatyk@amu.edu.pl

Abstract

Synthesis of multicomponent crystals offers a possibility for relatively straightforward tailoring of physicochemical properties of materials via modification of their composition. Still, despite their vast potential, they remain understudied at non-ambient conditions, missing out on possible structural and chemical effects induced by external stimuli such as temperature or pressure. In this work, high pressure was applied to trigger proton-transfer reaction in a cocrystal of glutaric acid and 4,4'-vinylenodipyridine, with the aim of investigating the relationship between the proton-transfer pressure and difference in the acidity of the coformers (ΔpK_a). Our combined IR spectroscopic and X-ray diffraction investigation, supported by DFT calculations, has confirmed that the reaction was successfully induced, with the double proton transfer completed at ≈4 GPa. The reaction is discussed in terms of the changes in the bands observed in IR spectra, as well as changes in the geometry of the carboxylic groups and hydrogen bond between the coformers. Presented results agree with the previous study on cocrystal of malonic acid and 4,4'-bipyridine, providing new data points for establishing a more precise relationship between proton-transfer pressure and ΔpK_a.

Keywords: cocrystal, high pressure, proton transfer, ΔpK_a rule

1. Introduction

Design and synthesis of novel multicomponent crystals, especially salts and cocrystals, has emerged as an important research area, as modification of the crystals' composition allows for tailoring of the properties of solid forms [1–8]. They play a particularly important role in the pharmaceutical industry [9], where synthesis of salts and cocrystals of Active Pharmaceutical Ingredients (APIs) is a well-established approach to obtain crystal forms of APIs of desired physicochemical properties such as improved bioavailability [10–12], stability [11,13] or processability [14,15].

The design of cocrystals and salts typically involves the analysis of the compatibility of the chemical components, where the tendency of molecules to form complementary intermolecular interactions and heterosynthons, as well as the ability to undergo proton

transfer reaction (for salt formation) increases likelihood of synthesis of the desired crystal form [16]. For these reasons, compounds which molecules will form a Brønsted-Lowry acid-base pair with the API are frequently selected for cocrystal and salt screening [17]. Moreover, the difference in the acidity and basicity of the two compounds is the determining factor behind that type of the multicomponent crystal that is formed (salt vs. cocrystal). According to the empirical ΔpK_a rule, when ΔpK_a ($\Delta pK_a = pK_{a[\text{protonated base}]} - pK_{a[\text{acid}]}$) is higher than 2 or 3, formation of a salt is expected [18]. Interestingly, similar limit ($\Delta pK_a > 4$) was observed based on the statistical analysis of approx. 6500 structures of ionised and non-ionised acid-base pairs [19] deposited in the Cambridge Structural Database (CSD) [20]. It was also established that structures of cocrystals dominate for ΔpK_a values lower than -1. Meanwhile, for ΔpK_a in -1 to 4 range, the prediction of the solid form is not possible, with salt and cocrystal structures in approx. 40:60 ratio. It was shown that for compounds belonging to this group structure can exist on salt-cocrystal continuum, where some proton transfer takes place but is not completed, and hydrogen cation is shared by two atoms [21]. It also needs to be noted, that those ΔpK_a limits can change depending on crystalline environment [22]. Indeed, significantly higher ΔpK_a value for salt preference was observed in case of the structures containing zwitterions.

Understanding the cocrystal-salt relationship and intermolecular proton transfer is important from the point of view of the stimuli-responsive materials, that utilize such process, that may have potential to find application in photoelectric devices, sensors or molecular computers [23]. Among the stimuli found to induce proton transfer in solid state are pressure and temperature [24–30]. However, in case of organic cocrystals, heating has limited use since it may lead to thermal decomposition of coformers and melting prior to achieving conditions required for the reaction to take place. Meanwhile, high-pressure conditions facilitate proton transfer by tuning the energy barrier for the reaction, achieved by reduction of the distance between proton donor and acceptor [31,32].

Unfortunately, the crystal structures of multicomponent crystals remain understudied under pressure, making only 36.26% of the high-pressure CSD subset, while their

population in the entire CSD is significantly higher (44.60%) – both values found for the CSD v.6.01 November 2025 [20]. Among those, the proton transfer reaction can be realized only in handful cases, due to their composition and relative positioning of the hydrogen donors and acceptors [33]. Although scarce, some examples of pressure-induced proton transfer in multicomponent crystals can be found in the literature, including: quinhydrone [25], 4,4'-bipyridinium squarate [24,34,35], oxalic acid dihydrate form α [36–38], cocrystals of phenazine and 2,3-di(2-pyridinyl)pyrazine with fluoranilic acid [39,40], cocrystal of 4-methylpyridine and pentachlorophenol [41], and cocrystal of 4,4'-bipyridine (BIPY) and malonic acid (MA) [33]. Based on those examples an inverse relationship between ΔpK_a and pressure required to induce proton transfer was revealed extending the ΔpK_a rule by adding additional parameter – pressure – to it [33]. These observations were also compared with the CSD deposits of multicomponent crystals previously investigated under pressure, where proton transfer should be expected based on the ΔpK_a value but was not reported. It turned out that in most cases such crystals contained molecules of amino acids, which would be in agreeament with statistical analysis of ambient-condition structures, where higher limits for salt formation were observed when zwitterions were present [22]. Still, the limited data did not allow to establish more precise relationship between the two parameters, and further studies of similar multicomponent systems are needed to increase the precision of these findings.

In this work a cocrystal (VIN·GLU) based on 4,4'-vinylenodipyridine (VIN) and glutaric acid (GLU) was investigated under high pressure using single crystal X-ray diffraction and IR spectroscopy. Due to the diprotic nature of the acid and bidentate nature of base molecules, and their alternating aggregation in the structure (Figure S1), two proton-transfer reactions are possible. Each of the reactions is associated with different ΔpK_a, with values calculated based on the literature pK_a data (Table S1) [42,43], for the transfer of the first and second proton equal 1.26 and -1.76, respectively (Scheme 1). According to the previously established relationship between ΔpK_a and pressure required to induce proton transfer [33], the cocrystal-to-monoprotonated salt and monoprotonated salt – to

– diprotonated salt transformation was estimated to occur between approx. 0.5-1.5 and 2.0-3.0 GPa, respectively.

The aim of this investigation was to validate our previous findings regarding proton-transfer pressure (p_{pt}) and ΔpK_a, as well as provide new data that would bring us closer to establishing more precise relationship between the two parameters, allowing for more accurate prediction of pressure required for salt formation for any Brønsted-Lowry acid-base.

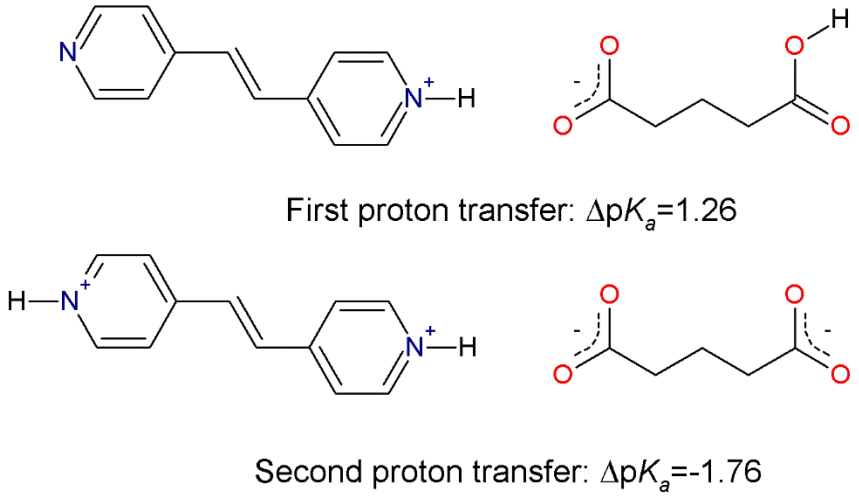

Scheme 1. Graphical representation of GLU and VIN acid-base pair after first and second proton transfer.

2. Experimental

2.1. Cocrystal synthesis

To receive single crystals, 36 mg of 4,4'-vinylenedipyridine and 28 mg of glutaric acid (ensuring 1:1 mol ratio) were dissolved in 1 ml of methanol, and left for slow evaporation. After several days a light-yellow crystal emerged. For bulk synthesis of VIN·GLU powder, 124 mg of VIN was mixed with 90 mg of GLU at the presence of 100 µL of methanol, using Retsch MM 400 ball mill, 10 ml steel jars, and two 5mm steel balls. Cocrystal synthesis was confirmed with powder X-ray diffraction (PXRD) analysis (Figure S2).

2.2. High pressure X-ray diffraction experiments

Single crystal of VIN·GLU was mounted in a diamond anvil cell (DAC) with effective opening angle of 112° (a one20 DAC design from Almax EasyLab), in 0.37 mm wide opening in a steel 0.25 mm thick gasket preindented to 0.15 mm. For experimental series A, crystal's position was fixed using epoxy glue (Figure S3) and Daphne 7575 oil was used as pressure transmitting medium (PTM). For experimental series B, cigarette filter fibres were used to prevent crystals from moving (Figure S4) and the MeOH:EtOH:H_2O mixture in 16:3:1 vol. ratio was used as PTM. In both cases pressure was measured based on the shift of ruby fluorescence line [44], using BETSA PRL spectrometer equipped in PhotonControl detector. The pressure was determined using IPPS-Ruby2020 gauge [45]. The combined uncertainty of the pressure measurement was established considering the accuracy of the used ruby scale (2.5%) and the accuracy of the measurement of the ruby fluorescence line (0.05 GPa). For series A crystal was measured on compression at 0.0001, 0.29(5), 0.71(5), 1.16(6), 1.62(6), 2.02(7), 2.67(8) GPa. The sample was then decompressed to 2.55(8) GPa and then subjected to further compression and measured at 2.82(9), 2.99(9), and 3.59(10) GPa. In case of sample crystal B, measurements were performed on compression at 0.20(5), 1.80(7), 3.06(9), 4.28(12), 4.51(12), 5.05(14) GPa, and on decompression at 4.04(11), 2.45(8), 0.82(5) GPa. For all measurements, a four-circle Bruker D8 Quest diffractometer equipped with Mo microfocus sealed tube, multilayer mirror monochromator and CPAD detector was used.

For data collection, *UB*-matrix determination, absorption correction, and data integration program APEX 6 was used [46]. Crystal structure was solved using intrinsic phasing with ShelXT [47], and non-spherically refined with NoSpherA2 [48] and Orca 6.0 [49,50], using Olex2 as an interface [51]. For the refinement a PBE method/def2-SVP basis set was applied, for normal integration accuracy. In case of sample crystals A and B all non-hydrogen atoms were refined anisotropically. For crystal A, position of all hydrogen atoms except acidic H-atom (H1) was fixed based on idealized geometry, while position of atom H1 was free to refine. In case of sample crystal B, position of all atoms (including hydrogen atoms) was refined. For crystallographic details for all structures see Tables S2 and S3. All crystal structures were deposited with the Cambridge Crystallographic Data Centre (No 2506656-2506675) and can be accessed free of

charge by filling out an online form at https://www.ccdc.cam.ac.uk/structures/. Additionally, CIF files were deposited in Zenodo repository.

2.3. IR measurements

For atmospheric pressure, the IR spectrum was recorded for a tablet made of powder VIN·GLU (received from ball-mill synthesis) and KBr. The experiment was performed at room temperature, in transmission mode (for 4000-400 cm^{-1} range) with Bruker FT-IR IFS 66/s spectrometer. The transmission spectrum was then converted to absorption spectrum (Figure S5).

For high-pressure experiments, powder sample of VIN·GLU mixed with dehydrated powder KBr was ground in approx. 1:4 vol ratio in agate mortar, and then loaded into 0.25mm wide opening in stainless steel gasket (preindented to 0.06 mm) placed in a membrane DAC. Ruby sphere was used for pressure measurement with ruby fluorescence method [44] and in-house made PRL spectrometer. The ruby scale established by Mao *et al.* [52], that allows to determine pressure with 6% uncertainty, was applied. Sample was measured in 500-5000 cm^{-1} range at 0.0001, 0.11(1), 0.21(1), 0.41(2), 0.68(4), 0.92(6), 1.08(6), 1.30(8), 1.52(9), 1.76(11), 2.09(13), 2.30(14), 2.62(16), 3.08(18), 3.6(2), 4.3(3), 4.6(3), 4.8(3), 5.4(3) and 6.1(4) GPa on compression and at 5.0(3), 4.0(2), 2.77(17), 1.30(8) and 0.0001 GPa on decompression (Figure S6), using Bruker Vertex 80v IR spectrometer. For data collection and initial analysis program OPUS [53] was used. Prior to the experiments, cell was loaded with powder anhydrous KBr and measured to record background used for further experiments.

2.4. DFT calculations

DFT calculations under static conditions have been performed using the Vienna Ab initio Simulation Package (VASP) [54] and the Projector Augmented Wave (PAW method) [55]. We use the Perdew-Burke exchange correlation functional [56] and the Grimme-D3 dispersion correction with Becke-Johnson damping function [57]. A planewave cut-off of 600 eV was chosen with a Gamma centered k-point mesh with a resolution of 0.25 $Å^{-1}$. The valence active space for C, N, O, H atoms was selected as 4, 5, 6, and 1 electron respectively. Vibrational properties at the gamma point were computed using the finite difference method implemented in the PHONOPY package

[58,59]. Intensities were computed using the SpectroscoPY code [60]. Energy and forces convergence thresholds were set at 10^{-9} eV and 0.005 eV·Å^{-1}.

To analyse the stability and the proton transfer of VIN·GLU three independent optimizations at each volume were performed maintaining the *C*2/*c*, *C*2 and *Cc* space groups to check symmetry rupture in the case of single proton transfer. For all space groups the following calculations were performed: starting with (i) the protons at the GLU, (ii) one proton transferred to the VIN and, (iii) two protons transferred. Vinet equations [61] of state were fitted to obtain the thermodynamic properties of each possible structure.

3. Results and discussion

VIN·GLU crystallizes in monoclinic crystal system, space group *C*2/*c* with half of VIN and GLU molecules in the asymmetric part of the unit cell [62]. On compression up to 5.05(14) GPa, VIN·GLU undergoes monotonic changes, showing 21.5% drop in unit-cell volume with no phase transition (Figure 1). Crystals of VIN·GLU show positive linear compressibility (PLC) along all three principal axes (Tables S4 and S5), however the compressibility calculated for sample crystal A and B differ slightly, which can be attributed to crystal A being emerged in an epoxy glue, which could affect its response to compression. Nevertheless, the highest and lowest PLC were observed for both sample crystals (A/B) in similar directions: 0.54***a***+0.84***c***/0.49***a***+0.87***c***, -0.49***a***+0.87***c***/-0.55***a***+0.83***c*** respectively (Tables S4, S5).

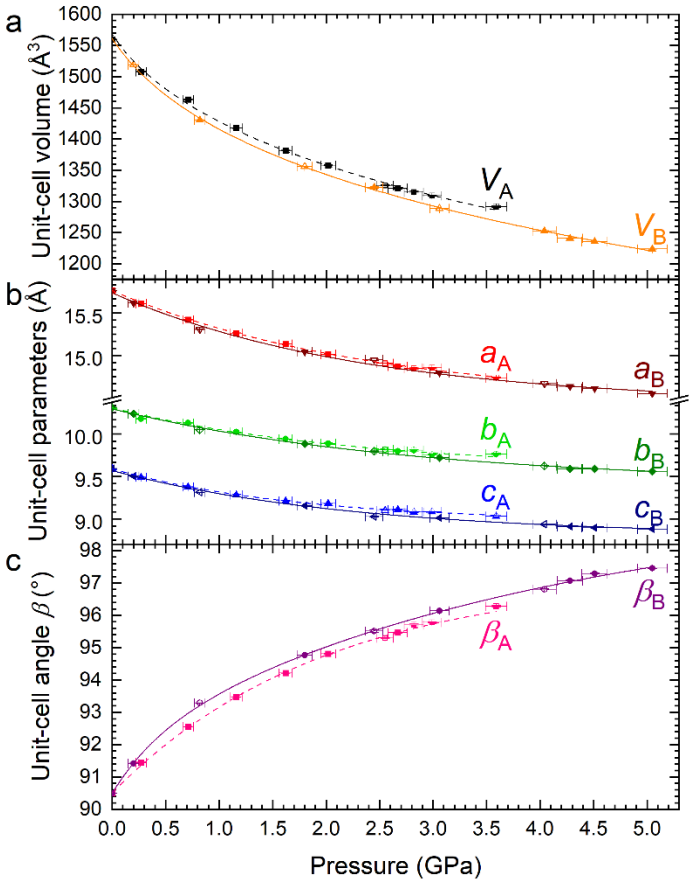

Figure 1. Pressure dependence of unit-cell volume (a), parameters (b) and *β* angle (c). Data collected for sample crystals A and B are shown separately, and are indicated by appropriate subscripts. Open symbols mark data collected on decompression of the sample crystals. For sample crystal A, half-full symbols mark data for sample compressed after initial decompression from 2.67 to 2.55 GPa. Curves in pane (a) represent 3rd order Birch–Murnaghan equation of state calculated with EosFit-7 [63,64] for each crystal separately (A: dashed black line; B: solid orange line); for details see Table S6. Curves fitted to data points for unit-cell parameters and angle *β* (see Tables S7, S8), dashed and solid for sample crystals A and B, respectively, are for guiding the eye only.

In case of sample crystal A, the pressure-dependence of carbon-oxygen bond length shows no clear trend, which might be attributed to the strain arising from the inability of the crystal to adapt when it is partially covered in glue. Still, however, a slight elongation of the carbonyl bond and shortening of a single C-O bond over the span of 3.61 GPa can be noticed

(Figure S7, Table S9). On the other hand, the changes in the carbon-oxygen bond lengths in structures determined for data collected for sample crystal B, are more consistent, showing shortening of the single carbon-oxygen bond and elongation of the double C=O bond up to approx. 4 GPa (Figure 2). In 4-5 GPa range the length of C-O and C=O bonds remains almost unaffected by compression. At the same time the distance between H-donor oxygen atom of GLU and H-acceptor nitrogen atom of VIN decreases continuously on crystals compression, until it drops below 2.50 Å at approx. 4 GPa, and becomes almost constant on further pressure increase up to 5 GPa (Figure 2, Table S10). For comparison, the O···N distance in BIPY·MA cocrystal after double proton transfer, at 3.33 GPa, was equal to 2.542(12)/2.593(13) Å [33], which is considerably higher. The observed values agree with the DFT calculations, where preference for the carbon-oxygen bonds consistent with double proton transfer were observed for pressure higher than 3.2 GPa (Figure S8). At the same time it has been shown that critical O···N distance of 2.51 Å is achieved at a pressure of 3.2 GPa regardless of the protonation state assumed in the calculations (Figure S9).

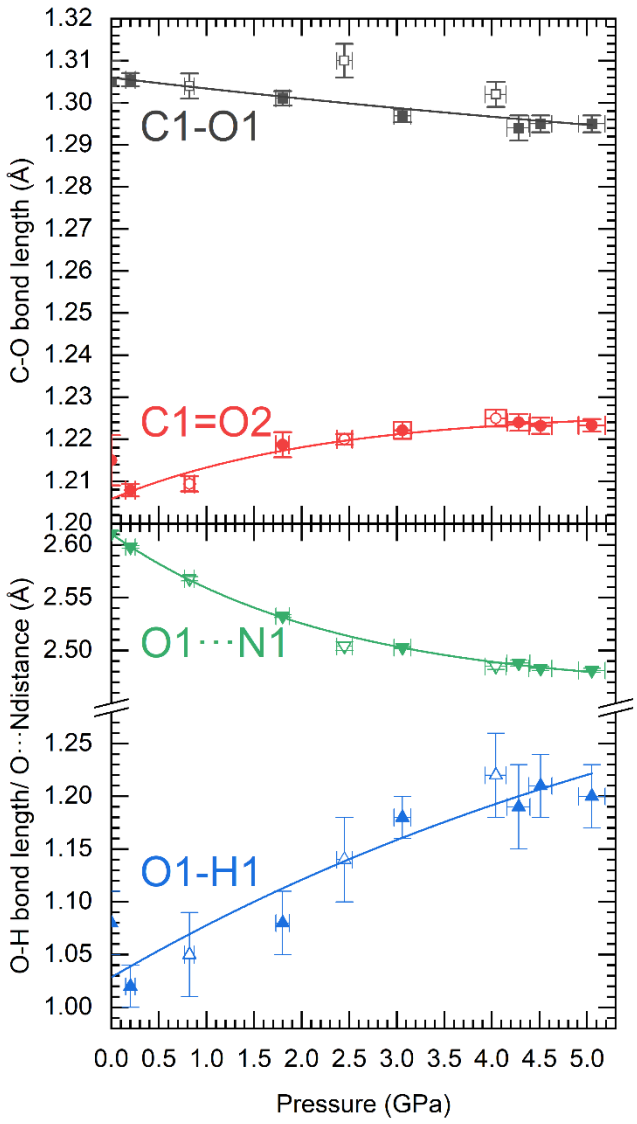

Figure 2. Pressure dependence of (a) the carbon-oxygen bond lengths in carboxylic groups of GLU (grey and red), and (b) O···N distance and oxygen-hydrogen bond length for the H-bond formed by GLU and VIN molecules (shown in green and blue, respectively). Data for sample crystal B are shown exclusively, and solid lines are for guiding the eye only. Open symbols mark data collected on decompression of the sample crystal.

As the position of acidic hydrogen atom was also refined, it was revealed that the length of the oxygen-hydrogen bond and the hydrogen—nitrogen distance also change with pressure, with the first elongating and the other decreasing. Yet again, the change can be observed up to approx. 4 GPa, and further compression to 5 GPa affects the interatomic distances only in slight

manner (Figure 2). Similar trend is observed for the theoretical bond lengths (Figure S10), with the pressure limit for double proton transfer of 3.2 GPa established.

These results of X-ray diffraction experiments and DFT calculations are consistent with the IR spectroscopic measurements. The effect of pressure on the O-H···N hydrogen bond can be noticed in the red shift of the band at approx. 1700 cm^{-1} in the IR spectra (Figures S6 and S12), a band associated with the stretching mode of the double carbon-oxygen bond. Usually, compression of the sample results in a blue shift, caused by shortening of the covalent bonds at high pressure, therefore the red shift signalizes the bond elongation with pressure, which is counterintuitive. However, red shift can be observed as a result of strengthening of the hydrogen bond or if deprotonation of the carboxylic group takes place. The steady change in the position of the band can signalize gradual strengthening of the hydrogen bond. This ultimately leads to deprotonation of GLU at approx. 4 GPa, associated with change in the nature of the carbon-oxygen bond from double to delocalized. Interestingly, above 4 GPa, the position of the band remains almost unchanged on further compression up to 6 GPa, except for a minimal blue shift, expected for pressure increase (Figure S12).

At the same time, major changes are observed in the 1100-1350 cm^{-1} region of the IR spectra (Figure 3a and S6). For most of the bands an expected blue shift is recorded, however, the band at approx. 1200 cm^{-1}, that can be assigned to stretching of the C-O bond, loses its intensity on pressure increase, and above 2 GPa the tracking of its shift is hindered (Figure 3a). Meanwhile, starting from 0.21(1) GPa, a band at approx. 3100 cm^{-1} begins to emerge, and it increases its intensity with compression (Figure 3b). This band can be assigned to stretching of N-H bond, where nitrogen has formal positive charge and the hydrogen atom is involved in the interaction with the deprotonated carboxylic group of the acid [65]. Although, only one band is initially visible in this region, and a pair of bands should be present (for symmetric and antisymmetric N-H stretching), its broad shape can indicate an unresolved band doublet. As pressure is increased further, the band appears to separate into two, which is visible the most in 3.6(2)-6.1(4) GPa range (Figure 3b). The emergence of the bands associated with proton transfer reaction between GLU and VIN was also observed in theoretically calculated IR spectra (Figures S13-S17).

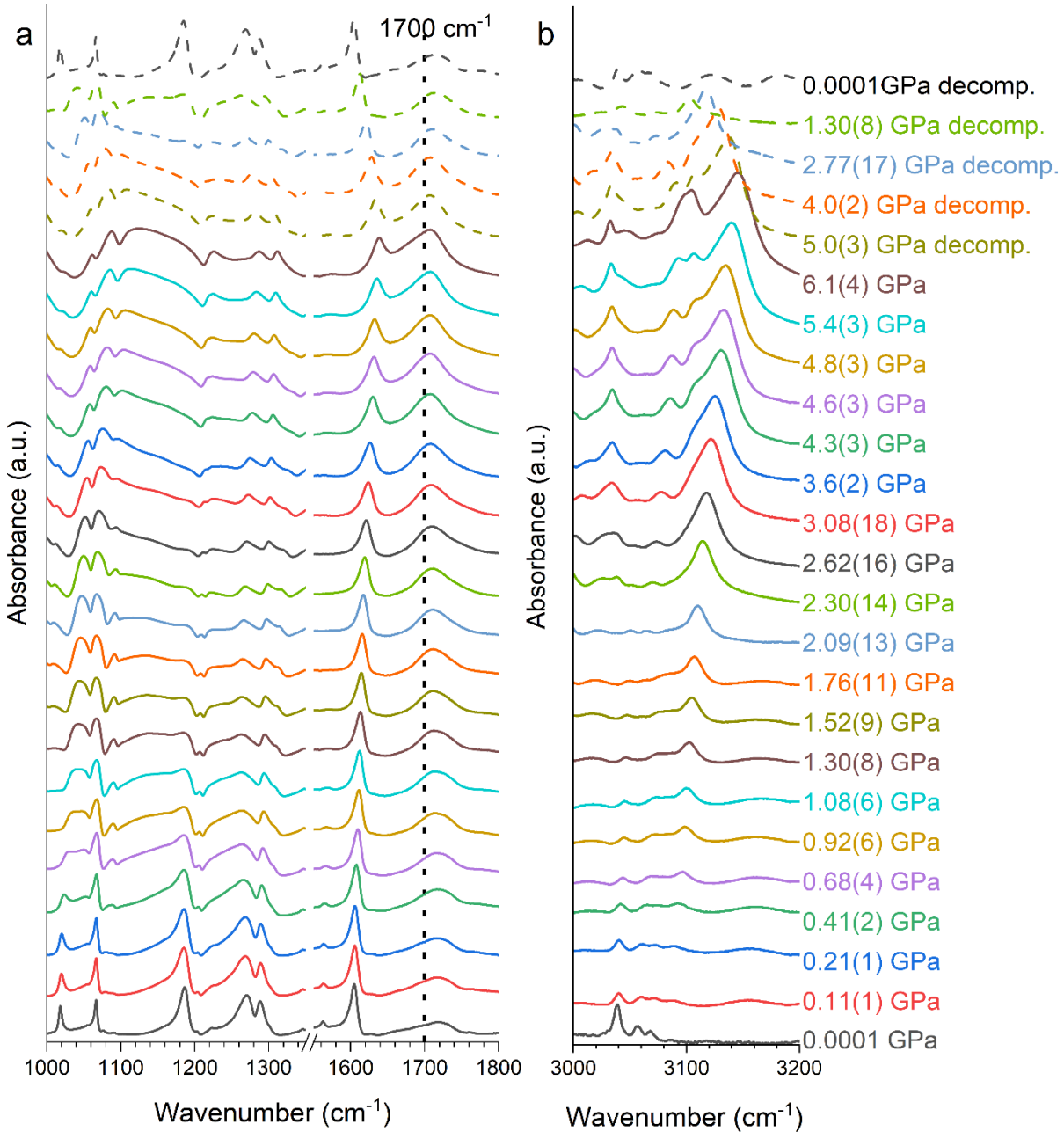

Figure 3. Magnification of crucial regions in IR spectra measured for VIN·GLU at varied pressure: (a) 1000-1400 cm^{-1} and 1560-1800 cm^{-1}; (b) 3000-3200 cm^{-1}. The pressure at which each spectrum was collected is listed to the right of the graph in pane (b), shown in corresponding colour. To facilitate observation of the shift of the band near 1700 cm^{-1}, a dotted vertical line was added. IR spectra collected for compressed and decompressed sample are shown with solid and dashed lines, respectively.

Interestingly, predicted IR spectra show a band at approximately 2000 cm^{-1} which was revealed to be associated with continuous "jumping" of the acidic hydrogen between oxygen atom of GLU and nitrogen atom of VIN, already at atmospheric pressure. This band cannot be observed in the experimentally measured IR spectra for the cocrystal at high pressure. Its position is near the region where the second order band of the DAC diamonds is observed, making its analysis impossible (Figure S6). Nevertheless, this DFT predicted IR band at 2000 cm^{-1} agrees with a previous study by Mukherjee *et al.* [66]. These authors proposed that for the carboxylic group H-bonded to pyridine moiety, a set of bands at approx. (1900, 2400)/500/1600 cm^{-1}, assigned respectively to νO–H/δas(CCC)PY + $\nu(HN)^{+}$/$\nu(C{=}C)_{Aromatic}$ modes, should be observed. The pair of bands at approx. 1900 and 2400 cm^{-1}, and the band at 500 cm^{-1} has been previously linked to the continuous proton migration between H-donor and acceptor of the hydrogen bond [66,67]. This is in agreement with the DFT calculations, which predicted "jumping" of the proton between GLU and VIN molecules already at atmospheric pressure, placing it on a salt-cocrystal continuum [21].

It is worth noting that the ΔpK_a value for the first proton transfer in VIN·GLU, equal 1.26 is lower compared to BIPY·MA cocrystal (1.99), which would suggest higher pressure should be required to induce the reaction. In case of BIPY·MA, DFT calculations revealed that the coexistence of the cocrystal and monoprotonated salt, that easily transform from one to the other, can be observed at pressure as low as 0.2 GPa and room temperature, as the activation energy for proton transfer was predicted to be below 1.6 $kJ{\cdot}mol^{-1}$ for molecular volume of 287.5 $Å^3$. Meanwhile, DFT calculations and IR spectroscopic experiments at atmospheric pressure suggest that continuous proton migration in VIN·GLU is initiated at pressure lower than in case of BIPY·MA, already at 0.1 MPa. Interestingly, the monoprotonated salt never becomes the preferred form in terms of energy (Figure S18), yet at approx. 1.4 GPa (i.e. molecular volume 345 $Å^3$) its energy is higher than that of cocrystal by only 0.02 eV (1.93 $kJ{\cdot}mol^{-1}$). The energy gap then decreases even more on further compression, up to pressure of approx. 2.2 GPa (corresponding to molecular volume of 333 $Å^3$), when the diprotonated salt becomes the energetically favoured form. When the results of DFT calculations are contrasted with experimental observations on the emergence of the band in IR spectrum at approx. 3100 cm^{-1} at 0.21(1) GPa, a 0.2-2.2 GPa range

can be considered a region where $VINH^+GLU^-$ and VIN·GLU coexist, and transition between them can be activated already at room temperature – a similar case to BIPY·MA.

Based on IR experiments the proton transfer in VIN·GLU is a continuous process, as observed in gradual emergence of the band at 3100 cm^{-1} and red shift of band at 1700 cm^{-1}. These changes continue up to pressure of 4 GPa, which corresponds to molecular volume of 314 $Å^3$. This coincides with the increase in the energy gap between cocrystal and $VINH_2^{2+}GLU^{2-}$, which for molecular volume of 320 $Å^3$ (corresponding to pressure of 3.2 GPa) is 0.04 eV (3.86 $kJ \cdot mol^{-1}$). Therefore, it can be inferred, that at 4 GPa, both proton reactions are completed and crystal is a diprotonated salt. If that pressure limit is considered alone, it is significantly higher than the proton-transfer pressure expected based on the inverse relationship of p_{pt} and ΔpK_a. However, according to DFT calculations, the $VINH_2^{2+}GLU^{2-}$ form becomes the preferred one already at pressure of 2.2 GPa, which agree with the expected pressure limit for double proton transfer between 2 and 3 GPa (Figure 4).

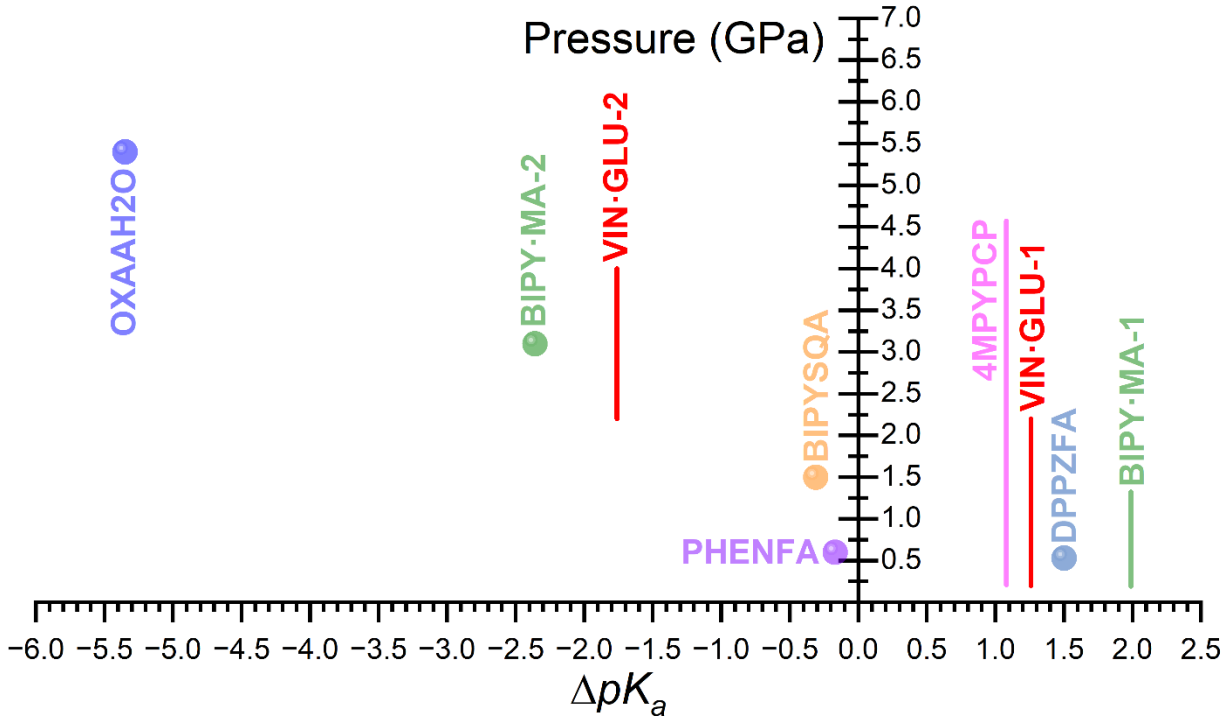

Figure 4. The p_{pt} in function of ΔpK_a for confirmed proton transfer reactions in multicomponent crystals, marked with dots (when single pressure value was reported) or with solid lines, when

pressure range was determined instead (BIPYMA-1), or when the proton-transfer pressure was not reported (4MPYPCP). Symbols and lines at 50% transparency mark previously analysed data [33], while red lines are for data for VIN·GLU crystal. The numbers 1 and 2 following acronyms reference the first and second proton transfer. The acronyms: OXAAH2O – oxalic acid dihydrate form α [36]; BIPYSQA – 4,4'-bipyridinium squarate [24,34]; PHENFA – cocrystal of phenazine with fluoranilic acid [39]; 4MPYPCP – cocrystal of 4-methylpyridine with pentachlorophenol [41]; DPPZFA – cocrystal of 2,3-di(2-pyridinyl)pyrazine with fluoranilic acid [40].

4. Conclusions

The pressure-induced proton transfer in VIN·GLU cocrystal was confirmed with X-ray diffraction and spectroscopic techniques, supported by DFT calculations. It was revealed that continuous "jumping" of the proton takes place already at atmospheric pressure, and a mixture of $VINH^+GLU^-$ and VIN·GLU forms exist in 0.2-2.2 GPa range. The diprotonated salt is stable at pressure above 2.2 GPa, however, the energy difference between all three forms is negligible at that pressure. Only when pressure of 3.2 GPa is reached the preference for $\mathrm{VINH_2^{2+}GLU^{2-}}$becomes significant. Still, a further compression to 4 GPa is required to complete the reaction. The process is reversible, with proton transfer being reverted on decompression. However, this case differs compared to BIPY·MA in several aspects. Firstly, in VIN·GLU the reaction takes place monotonically when crystal is compressed , and no phase transition is observed. Although in both cocrystals we observe a pressure range where neutral and monoprotonated forms coexist, in BIPY·MA the second proton transfer was observed at single pressure of 3.1 GPa, while in VIN·GLU the proton transfer appears to be a continuous process. Lastly, a significant difference in the critical distance between the donor and acceptor of the hydrogen bond for BIPY·MA and VIN·GLU can be noticed. In the first case, the double proton transfer took place when the oxygen—nitrogen distance decreased to approx. 2.55 Å. Meanwhile, completion of double proton transfer in VIN·GLU was associated with the distance of 2.485(3) Å.

Our results agree reasonably with previously observed relationship between proton-transfer pressure and ΔpK_a, according to which, the pressure required for the first and second proton transfer for VIN·GLU should be approx. 0.5-1 and 1.5-2.5 GPa, respectively. Although, the

limits found by us differ from this estimation, the expected range falls entirely in the experimentally established range of 0.2-2.2 GPa for the first proton transfer, while partial overlap of expected and experimental pressure ranges is observed for the second proton transfer (with deprotonated salt becoming energetically favourable at 2.2 GPa). Still, the inversed relationship between proton-transfer pressure and ΔpK_a is preserved, in agreement with the extended ΔpK_a rule.

Author Contributions

E. P-K: conceptualization, investigation, formal analysis, resources, writing (original draft, review and editing), visualization, supervision, project administration, funding acquisition; M.K: crystallization, formal analysis, writing- review and editing; M.W.: sample preparation, visualization; F. I-R.: DFT calculations, formal analysis, visualization, writing- review and editing; A. L.: calculations, formal analysis, visualization, writing- review and editing; S. R.: investigation (support of IR experiments), initial IR data treatment, writing- review and editing; R. B.: funding acquisition, writing- review and editing; J. M. R.: funding acquisition, writing- review and editing.

Funding

E.P-K., M.K. and M.W kindly acknowledge funding from National Science Centre, Poland (Grant No. UMO-2020/39/D/ST4/00260). E.P-K. also acknowledges funding from ID-UB scheme at Adam Mickiewicz University (Grant No. 165/07/POB3/0015). A.L., F.I-R. and J.M.R. acknowledge funding from Spanish MICIU/AEI/10.13039/501100011033 and European Union Next Generation EU/PRTR (PID2021-122585-NB-C21-2). R). J.M.R. also acknowledges the Principality of Asturias, the project IDE/2024/000726 co-financed by EU FEDER funds. S.R and R.B kindly acknowledge funding provided by the project “Next Generation EU, Integrated infrastructure initiative in Photonic and Quantum Sciences” IPHOQS cup: B53C22001750006

Data availability

Raw SCXRD data will be made available on request. The cif files (No 2506656-2506675) containing crystal structure information are deposited with Cambridge Crystallographic Data Centre and can

be accessed at https://www.ccdc.cam.ac.uk/structures/. The cif files and IR data were also deposited in Zenodo repository.

References

[1] M.R. Bryce, Recent progress on conducting organic charge-transfer salts, Chem. Soc. Rev. 20 (1991) 355–390. https://doi.org/10.1039/CS9912000355.

[2] L. Sun, W. Zhu, F. Yang, B. Li, X. Ren, X. Zhang, W. Hu, Molecular cocrystals: design, charge-transfer and optoelectronic functionality, Phys. Chem. Chem. Phys. 20 (2018) 6009–6023. https://doi.org/10.1039/C7CP07167A.

[3] G. Xing, T. Yan, S. Das, T. Ben, S. Qiu, Synthesis of Crystalline Porous Organic Salts with High Proton Conductivity, Angew Chem. Int. Ed. 57 (2018) 5345–5349. https://doi.org/10.1002/anie.201800423.

[4] S. Yu, G.-L. Xing, L.-H. Chen, T. Ben, B.-L. Su, Crystalline Porous Organic Salts: From Micropore to Hierarchical Pores, Advanced Materials 32 (2020) 2003270. https://doi.org/10.1002/adma.202003270.

[5] M. Jiang, C. Zhen, S. Li, X. Zhang, W. Hu, Organic Cocrystals: Recent Advances and Perspectives for Electronic and Magnetic Applications, Frontiers in Chemistry 9 (2021). https://www.frontiersin.org/articles/10.3389/fchem.2021.764628 (accessed August 28, 2023).

[6] C. Wang, T. Yan, G. Xing, S. Bailey, C. Lambert, P. Fayon, A. Trewin, T. Ben, Electron and proton conducting framework organic salt single crystals, Journal of Solid State Chemistry 308 (2022) 122903. https://doi.org/10.1016/j.jssc.2022.122903.

[7] T. Xu, B. Wu, L. Hou, Y. Zhu, F. Sheng, Z. Zhao, Y. Dong, J. Liu, B. Ye, X. Li, L. Ge, H. Wang, T. Xu, Highly Ion-Permselective Porous Organic Cage Membranes with Hierarchical Channels, J. Am. Chem. Soc. 144 (2022) 10220–10229. https://doi.org/10.1021/jacs.2c00318.

[8] S. Zhang, J. Fu, S. Das, K. Ye, W. Zhu, T. Ben, Crystalline Porous Organic Salt for Ultrarapid Adsorption/Desorption-Based Atmospheric Water Harvesting by Dual Hydrogen Bond System, Angew Chem. Int. Ed. 61 (2022) e202208660. https://doi.org/10.1002/anie.202208660.

[9] O.D. Putra, H. Uekusa, Pharmaceutical Multicomponent Crystals: Structure, Design, and Properties, in: M. Sakamoto, H. Uekusa (Eds.), Advances in Organic Crystal Chemistry: Comprehensive Reviews 2020, Springer, Singapore, 2020: pp. 153–184. https://doi.org/10.1007/978-981-15-5085-0_9.

[10] M.L. Cheney, N. Shan, E.R. Healey, M. Hanna, L. Wojtas, M.J. Zaworotko, V. Sava, S. Song, J.R. Sanchez-Ramos, Effects of Crystal Form on Solubility and Pharmacokinetics: A Crystal Engineering Case Study of Lamotrigine, Cryst. Growth Des. 10 (2010) 394–405. https://doi.org/10.1021/cg901010v.

[11] K. Sigfridsson, M.-L. Ulvinge, L. Svensson, A.-K. Granath, A case study where pharmaceutical salts were used to address the issue of low in vivo exposure, Drug Development and Industrial Pharmacy 45 (2019) 202–211. https://doi.org/10.1080/03639045.2018.1529184.

[12] L. Li, X.-H. Yin, K.-S. Diao, Improving the solubility and bioavailability of anti-hepatitis B drug PEC via PEC–fumaric acid cocrystal, RSC Adv. 10 (2020) 36125–36134. https://doi.org/10.1039/D0RA06608G.

[13] L. Liu, J.-R. Wang, X. Mei, Enhancing the stability of active pharmaceutical ingredients by the cocrystal strategy, CrystEngComm 24 (2022) 2002–2022. https://doi.org/10.1039/D1CE01327K.

[14] S. Karki, T. Friščić, L. Fábián, P.R. Laity, G.M. Day, W. Jones, Improving Mechanical Properties of Crystalline Solids by Cocrystal Formation: New Compressible Forms of Paracetamol, Advanced Materials 21 (2009) 3905–3909. https://doi.org/10.1002/adma.200900533.
[15] P. Sanphui, M.K. Mishra, U. Ramamurty, G.R. Desiraju, Tuning Mechanical Properties of Pharmaceutical Crystals with Multicomponent Crystals: Voriconazole as a Case Study, Mol. Pharmaceutics 12 (2015) 889–897. https://doi.org/10.1021/mp500719t.
[16] D.C. Sakhiya, C.H. Borkhataria, A review on advancement of cocrystallization approach and a brief on screening, formulation and characterization of the same, Heliyon 10 (2024) e29057. https://doi.org/10.1016/j.heliyon.2024.e29057.
[17] A. Karagianni, M. Malamatari, K. Kachrimanis, Pharmaceutical Cocrystals: New Solid Phase Modification Approaches for the Formulation of APIs, Pharmaceutics 10 (2018) 18. https://doi.org/10.3390/pharmaceutics10010018.
[18] P.H. Stahl, C.G. Wermuth, Handbook of Pharmaceutical Salts: Properties, Selection, and Use, VHCA : Wiley-VCH, Weinheim, New York, 2002. https://www.loc.gov/catdir/toc/wiley031/2002510983.html (accessed August 28, 2023).
[19] A.J. Cruz-Cabeza, Acid-Base Crystalline Complexes and the pKa Rule, CrystEngComm 14 (2012) 6362–6365. https://doi.org/10.1039/C2CE26055G.
[20] C.R. Groom, I.J. Bruno, M.P. Lightfoot, S.C. Ward, The Cambridge Structural Database, Acta Cryst B 72 (2016) 171–179. https://doi.org/10.1107/S2052520616003954.
[21] S.L. Childs, G.P. Stahly, A. Park, The Salt−Cocrystal Continuum: The Influence of Crystal Structure on Ionization State, Mol. Pharmaceutics 4 (2007) 323–338. https://doi.org/10.1021/mp0601345.
[22] A.J. Cruz-Cabeza, M. Lusi, H.P. Wheatcroft, A.D. Bond, The Role of Solvation in Proton Transfer Reactions: Implications for Predicting Salt/Co-crystal Formation Using the ΔpKa Rule, Faraday Discuss. 235 (2022) 446–466. https://doi.org/10.1039/D1FD00081K.
[23] Y. Wang, Y.-M. Zhang, S.X.-A. Zhang, Stimuli-Induced Reversible Proton Transfer for Stimuli-Responsive Materials and Devices, Acc. Chem. Res. 54 (2021) 2216–2226. https://doi.org/10.1021/acs.accounts.1c00061.
[24] D.M.S. Martins, D.S. Middlemiss, C.R. Pulham, C.C. Wilson, M.T. Weller, P.F. Henry, N. Shankland, K. Shankland, W.G. Marshall, R.M. Ibberson, K. Knight, S. Moggach, M. Brunelli, C.A. Morrison, Temperature- and Pressure-Induced Proton Transfer in the 1:1 Adduct Formed between Squaric Acid and 4,4'-Bipyridine, J. Am. Chem. Soc. 131 (2009) 3884–3893. https://doi.org/10.1021/ja8082973.
[25] T. Mitani, G. Saito, H. Urayama, Cooperative Phenomena Associated with Electron and Proton Transfer in Quinhydrone Charge-Transfer Crystal, Phys. Rev. Lett. 60 (1988) 2299–2302. https://doi.org/10.1103/PhysRevLett.60.2299.
[26] M. Szafrański, A. Katrusiak, Short-Range Ferroelectric Order Induced by Proton Transfer-Mediated Ionicity, J. Phys. Chem. B 108 (2004) 15709–15713. https://doi.org/10.1021/jp047172t.
[27] M.K. Bhunia, S.K. Das, A. Bhaumik, Temperature induced proton transfer in a hydrogen bonded supramolecule, Chem. Phys. Lett. 498 (2010) 145–150. https://doi.org/10.1016/j.cplett.2010.08.057.
[28] W. Cai, A. Katrusiak, Pressure effects on H-ordering in hydrogen bonds and interactions in benzoic acid, CrystEngComm 14 (2012) 4420–4424. https://doi.org/10.1039/C2CE25128K.
[29] B. Yu, Y. Wang, L. Wang, X. Tan, Y.-M. Zhang, K. Wang, M. Li, B. Zou, S.X.-A. Zhang, Spontaneous proton transfer in a series of amphoteric molecules under hydrostatic pressure, Phys. Chem. Chem. Phys. 21 (2019) 17696–17702. https://doi.org/10.1039/C9CP02445J.
[30] M. Tadokoro, M. Itoh, R. Nishimura, K. Sekiguchi, N. Hoshino, H. Kamebuchi, J. Miyazaki, F. Kobayashi, M. Mizuno, T. Akutagawa, Proton Conduction at High Temperature in High-Symmetry

Hydrogen-Bonded Molecular Crystals of Ru^{III} Complexes with Six Imidazole-Imidazolate Ligands, Chemistry – A European Journal 28 (2022) e202201397. https://doi.org/10.1002/chem.202201397.
[31] L.I. Krishtalik, The Mechanism of Proton Transfer: An Outline, Biochimica et Biophysica Acta (BBA) - Bioenergetics 1458 (2000) 6–27. https://doi.org/10.1016/S0005-2728(00)00057-8.
[32] D. Kurzydłowski, Potential Energy Barrier for Proton Transfer in Compressed Benzoic Acid, RSC Adv. 12 (2022) 11436–11441. https://doi.org/10.1039/D2RA01736A.
[33] E. Patyk-Kaźmierczak, F. Izquierdo-Ruiz, A. Lobato, M. Kaźmierczak, I. Moszczyńska, A. Olejniczak, J.M. Recio, The curious case of proton migration under pressure in the malonic acid and 4,4'-bi-pyridine cocrystal, IUCrJ 11 (2024) 168–181. https://doi.org/10.1107/S2052252524000344.
[34] M.T. Reetz, S. Höger, K. Harms, Proton-Transfer-Dependent Reversible Phase Changes in the 4,4'-Bipyridinium Salt of Squaric Acid, Angew Chem. Int. Ed. 33 (1994) 181–183. https://doi.org/10.1002/anie.199401811.
[35] Z. Ma, J. Li, C. Liu, C. Sun, M. Zhou, High Pressure Spectroscopic Investigation on Proton Transfer in Squaric Acid and 4,4'-Bipyridine Co-crystal, Sci Rep 7 (2017) 4677. https://doi.org/10.1038/s41598-017-04980-3.
[36] N. Casati, P. Macchi, A. Sironi, Hydrogen Migration in Oxalic Acid Di-hydrate at High Pressure?, Chem. Commun. (2009) 2679–2681. https://doi.org/10.1039/B823458B.
[37] P. Macchi, N. Casati, W.G. Marshall, A. Sironi, The α and β forms of oxalic acid di-hydrate at high pressure: a theoretical simulation and a neutron diffraction study, CrystEngComm 12 (2010) 2596–2603. https://doi.org/10.1039/C002471F.
[38] H. Bhatt, A.K. Mishra, C. Murli, A.K. Verma, N. Garg, M.N. Deo, S.M. Sharma, Proton transfer aiding phase transitions in oxalic acid dihydrate under pressure, Phys. Chem. Chem. Phys. 18 (2016) 8065–8074. https://doi.org/10.1039/C5CP07442H.
[39] R. Kumai, S. Horiuchi, J. Fujioka, Y. Tokura, Ferroelectricity and Pressure-Induced Phenomena Driven by Neutral Ionic Valence Instability of Acid–Base Supramolecules, J. Am. Chem. Soc. 134 (2012) 1036–1046. https://doi.org/10.1021/ja208113p.
[40] S. Horiuchi, R. Kumai, Y. Tokura, High-Temperature and Pressure-Induced Ferroelectricity in Hydrogen-Bonded Supramolecular Crystals of Anilic Acids and 2,3-Di(2-pyridinyl)pyrazine, J. Am. Chem. Soc. 135 (2013) 4492–4500. https://doi.org/10.1021/ja400318v.
[41] N.P. Funnell, D.R. Allan, A.G.P. Maloney, R.I. Smith, C.J.G. Wilson, S. Parsons, Suppression of isotopic polymorphism, CrystEngComm 23 (2021) 769–776. https://doi.org/10.1039/D0CE01636E.
[42] G. Beggiato, G. Favaro, U. Mazzucato, Acid-base equilibria of dipyridylethylenes studied by absorption and fluorescence spectrometry, Journal of Heterocyclic Chemistry 7 (1970) 583–587. https://doi.org/10.1002/jhet.5570070317.
[43] E. Boschmann, R.D. Miller, Influence of sulfur groups on carboxylic acid strengths, Tetrahedron 74 (2018) 2617–2619. https://doi.org/10.1016/j.tet.2018.04.007.
[44] R.A. Forman, G.J. Piermarini, J.D. Barnett, S. Block, Pressure Measurement Made by the Utilization of Ruby Sharp-Line Luminescence, Science 176 (1972) 284–285. https://doi.org/10.1126/science.176.4032.284.
[45] G. Shen, Y. Wang, A. Dewaele, C. Wu, D.E. Fratanduono, J. Eggert, S. Klotz, K.F. Dziubek, P. Loubeyre, O.V. Fat'yanov, P.D. Asimow, T. Mashimo, R.M.M. Wentzcovitch, other members of the I. task group, Toward an international practical pressure scale: A proposal for an IPPS ruby gauge (IPPS-Ruby2020), High Pressure Research (2020). https://www.tandfonline.com/doi/full/10.1080/08957959.2020.1791107 (accessed December 30, 2025).
[46] Bruker AXS Inc., APEX6 v.2024.9-0., (2024).
[47] G.M. Sheldrick, SHELXT – Integrated Space-Group and Crystal-Structure Determination, Acta Cryst A 71 (2015) 3–8. https://doi.org/10.1107/S2053273314026370.

[48] F. Kleemiss, O.V. Dolomanov, M. Bodensteiner, N. Peyerimhoff, L. Midgley, L.J. Bourhis, A. Genoni, L.A. Malaspina, D. Jayatilaka, J.L. Spencer, F. White, B. Grundkötter-Stock, S. Steinhauer, D. Lentz, H. Puschmann, S. Grabowsky, Accurate Crystal Structures and Chemical Properties from NoSpherA2, Chem. Sci. 12 (2021) 1675–1692. https://doi.org/10.1039/D0SC05526C.
[49] F. Neese, The ORCA program system, WIREs Computational Molecular Science 2 (2012) 73–78. https://doi.org/10.1002/wcms.81.
[50] F. Neese, Software Update: The ORCA Program System—Version 6.0, WIREs Computational Molecular Science 15 (2025) e70019. https://doi.org/10.1002/wcms.70019.
[51] O.V. Dolomanov, L.J. Bourhis, R.J. Gildea, J.A.K. Howard, H. Puschmann, OLEX2: A Complete Structure Solution, Refinement and Analysis Program, J. Appl. Crystallogr. 42 (2009) 339–341. https://doi.org/10.1107/S0021889808042726.
[52] H.K. Mao, P.M. Bell, J.W. Shaner, D.J. Steinberg, Specific volume measurements of Cu, Mo, Pd, and Ag and calibration of the ruby R1 fluorescence pressure gauge from 0.06 to 1 Mbar, Journal of Applied Physics 49 (1978) 3276–3283. https://doi.org/10.1063/1.325277.
[53] Bruker Optics GmbH: & CO, OPUS, (2023).
[54] G. Kresse, J. Furthmüller, Efficiency of ab-initio total energy calculations for metals and semiconductors using a plane-wave basis set, Computational Materials Science 6 (1996) 15–50. https://doi.org/10.1016/0927-0256(96)00008-0.
[55] P.E. Blöchl, Projector augmented-wave method, Phys. Rev. B 50 (1994) 17953–17979. https://doi.org/10.1103/PhysRevB.50.17953.
[56] J.P. Perdew, K. Burke, M. Ernzerhof, Generalized Gradient Approximation Made Simple, Phys. Rev. Lett. 77 (1996) 3865–3868. https://doi.org/10.1103/PhysRevLett.77.3865.
[57] S. Grimme, J. Antony, S. Ehrlich, H. Krieg, A consistent and accurate ab initio parametrization of density functional dispersion correction (DFT-D) for the 94 elements H-Pu, J. Chem. Phys. 132 (2010) 154104. https://doi.org/10.1063/1.3382344.
[58] A. Togo, L. Chaput, T. Tadano, I. Tanaka, Implementation strategies in phonopy and phono3py, J. Phys.: Condens. Matter 35 (2023) 353001. https://doi.org/10.1088/1361-648X/acd831.
[59] J. Ulstrup, C.O. Östman, T.G. Strand, R. Stølevik, G. Borch, J.C. Craig, The Influence of Some Organic pi-Electron Systems on the Rate of the Electron Transfer Reaction between Thallium(III) and Iron(II) in Aqueous Perchloric Acid., Acta Chem. Scand. 23 (1969) 3091–3109. https://doi.org/10.3891/acta.chem.scand.23-3091.
[60] J.M. Skelton, L.A. Burton, A.J. Jackson, F. Oba, S.C. Parker, A. Walsh, Lattice dynamics of the tin sulphides SnS2, SnS and Sn2S3: vibrational spectra and thermal transport, Phys. Chem. Chem. Phys. 19 (2017) 12452–12465. https://doi.org/10.1039/C7CP01680H.
[61] P. Vinet, J.R. Smith, J. Ferrante, J.H. Rose, Temperature effects on the universal equation of state of solids, Phys. Rev. B 35 (1987) 1945–1953. https://doi.org/10.1103/PhysRevB.35.1945.
[62] D.R. Weyna, T. Shattock, P. Vishweshwar, M.J. Zaworotko, Synthesis and Structural Characterization of Cocrystals and Pharmaceutical Cocrystals: Mechanochemistry vs Slow Evaporation from Solution, Crystal Growth & Design 9 (2009) 1106–1123. https://doi.org/10.1021/cg800936d.
[63] R.J. Angel, M. Alvaro, J. Gonzalez-Platas, EosFit7c and a Fortran module (library) for equation of state calculations, Zeitschrift für Kristallographie - Crystalline Materials 229 (2014) 405–419. https://doi.org/10.1515/zkri-2013-1711.
[64] J. Gonzalez-Platas, M. Alvaro, F. Nestola, R. Angel, EosFit7-GUI: a new graphical user interface for equation of state calculations, analyses and teaching, J Appl Cryst 49 (2016) 1377–1382. https://doi.org/10.1107/S1600576716008050.

[65] A. Sediki, L.C. Snoek, M.-P. Gaigeot, N–H+ vibrational anharmonicities directly revealed from DFT-based molecular dynamics simulations on the Ala7H+ protonated peptide, International Journal of Mass Spectrometry 308 (2011) 281–288. https://doi.org/10.1016/j.ijms.2011.06.016.
[66] A. Mukherjee, S. Tothadi, S. Chakraborty, S. Ganguly, G.R. Desiraju, Synthon identification in co-crystals and polymorphs with IR spectroscopy. Primary amides as a case study, CrystEngComm 15 (2013) 4640–4654. https://doi.org/10.1039/C3CE40286J.
[67] S. Kong, I.G. Shenderovich, M.V. Vener, Density Functional Study of the Proton Transfer Effect on Vibrations of Strong (Short) Intermolecular O−H···N/O−···H−N+ Hydrogen Bonds in Aprotic Solvents, J. Phys. Chem. A 114 (2010) 2393–2399. https://doi.org/10.1021/jp911694r.